Supplementary Information (SI) for Physical Chemistry Chemical Physics.

Inverse Design of ZIFs through Artificial Intelligence Methods.

Panagiotis Krokidas[*1], Michael Kainourgiakis,[2] Theodore Steriotis,[3] George Giannakopoulos[1,4]

[1]Institute of Informatics & Telecommunications, National Center for Scientific Research "Demokritos", 15341 Agia Paraskevi Attikis, Greece

[2]Institute of Nuclear & Radiological Sciences & Technology, Energy & Safety, NCSR 'Demokritos', 15341 Agia Paraskevi Attikis, Greece

[3]Institute of Nanoscience and Nanotechnology, National Center for Scientific Research "Demokritos", 15341 Agia Paraskevi Attikis, Greece

[4]SciFY PNPC, 27, Neapoleos Str., 15341 Agia Paraskevi, Greece

[*]Corresponding author at p.krokidas@iit.demokritos.gr

1. The ZIFs

Table S1. The ZIFs of our database.

	Name	Metal	Linker	Functional Group
1	ZIF-8	Zn	mIm	$-CH_3$
2	ZIF-67	Co	mIm	$-CH_3$
3	CdIF-1	Cd	mIm	$-CH_3$
4	BeIF-1	Be	mIm	$-CH_3$
5	Cu-ZIF-8	Cu	mIm	$-CH_3$
6	Mg-ZIF-8	Mg	mIm	$-CH_3$
7	Mn-ZIF-8	Mn	mIm	$-CH_3$
8	ZIF-8-Br	Zn	mIm	-Br
9	Co-ZIF-8-Br	Co	mIm	-Br
10	ZIF-8-Cl	Zn	mIm	-Cl
11	ZIF-8-Im_1	Zn	mIm/mIm/Im	$-CH_3/-CH_3/-H$
12	ZIF-8-Im_2	Zn	mIm/Im/Im	$-CH_3/-H/-H$

13	ZIF-8-Im_3	Zn	Im/Im/Im	-H/-H/-H
14	ZIF-7-8	Zn	mIm/mIm/bIm	-CH_3/-CH_3/-H
15	Co-ZIF-7-8	Co	mIm/mIm/bIm	-CH_3/-CH_3/-H
16	Be-ZIF-7-8	Be	mIm/mIm/bIm	-CH_3/-CH_3/-H
17	Cu-ZIF-7-8	Cu	mIm/mIm/bIm	-CH_3/-CH_3/-H
18	Mg-ZIF-7-8	Mg	mIm/mIm/bIm	-CH_3/-CH_3/-H
19	Mn-ZIF-7-8	Mn	mIm/mIm/bIm	-CH_3/-CH_3/-H
20	ZIF-7-8-Cl	Zn	mIm/mIm/bIm	-CH_3/-CH_3/-Cl
21	ZIF-7-8-Br	Zn	mIm/mIm/bIm	-CH_3/-CH_3/-Br
22	ZIF-7-8-I	Zn	mIm/mIm/bIm	-CH_3/-CH_3/-F
23	ZIF-7-8-F	Zn	mIm/mIm/bIm	-CH_3/-CH_3/-Cl
24	Cd-ZIF-7-8-Cl	Cd	mIm/mIm/bIm	-CH_3/-CH_3/-Br
25	Cd-ZIF-7-8-Br	Cd	mIm/mIm/bIm	-CH_3/-CH_3/-Br
26	Co-ZIF-7-8-Cl	Co	mIm/mIm/bIm	-CH_3/-CH_3/-Cl
27	Co-ZIF-7-8-F	Co	mIm/mIm/bIm	-CH_3/-CH_3/-F
28	Co-ZIF-7-8-I	Co	mIm/mIm/bIm	-CH_3/-CH_3/-I
29	Be-ZIF-7-8-F	Be	mIm/mIm/bIm	-CH_3/-CH_3/-F
30	Be-ZIF-7-8-I	Be	mIm/mIm/bIm	-CH_3/-CH_3/-I
31	Cu-ZIF-7-8-F	Cu	mIm/mIm/bIm	-CH_3/-CH_3/-F
32	Cu-ZIF-7-8-Cl	Cu	mIm/mIm/bIm	-CH_3/-CH_3/-Cl
33	Cu-ZIF-7-8-Br	Cu	mIm/mIm/bIm	-CH_3/-CH_3/-Br
34	Cu-ZIF-7-8-I	Cu	mIm/mIm/bIm	-CH_3/-CH_3/-I
35	Mg-ZIF-7-8-Br	Mg	mIm/mIm/bIm	-CH_3/-CH_3/-Br
36	Mg-ZIF-7-8-I	Mg	mIm/mIm/bIm	-CH_3/-CH_3/-I
37	Mn-ZIF-7-8-Br	Mn	mIm/mIm/bIm	-CH_3/-CH_3/-Br
38	Mn-ZIF-7-8-I	Mn	mIm/mIm/bIm	-CH_3/-CH_3/-I
39	Cd-ZIF-7-8-I	Cd	mIm/mIm/bIm	-CH_3/-CH_3/-I
40	Tetrz-ZIF-8	Zn	tetrz	-CH_3

41	Co-Tetrz-ZIF-8	Co	Tetrz	$-CH_3$
42	Be-Tetrz-ZIF-8	Be	Tetrz	$-CH_3$
43	Cu-Tetrz-ZIF-8	Cu	Tetrz	$-CH_3$
44	Tetrz-ZIF-8-NH_2	Zn	Tetrz	$-NH_2$
45	Be-Tetrz-ZIF-8-NH_2	Be	Tetrz	$-NH_2$
46	Co-Tetrz-ZIF-8-NH_2	Co	Tetrz	$-NH_2$
47	dClm-ZIF-8	Zn	dClm	$-CH_3$
48	Co-dClm-ZIF-8	Co	dClm	$-CH_3$
49	Be-dClm-ZIF-8	Be	dClm	$-CH_3$
50	Cd-dClm-ZIF-8	Cd	dClm	$-CH_3$
51	Mg-dClm-ZIF-8	Mg	dClm	$-CH_3$
52	Cu-dClm-ZIF-8	Cu	dClm	$-CH_3$
53	dFm-ZIF-8	Zn	dFm	$-CH_3$
54	Co-dFm-ZIF-8	Co	dFm	$-CH_3$
55	Cd-dFm-ZIF-8	Cd	dFm	$-CH_3$
56	Mg-dFm-ZIF-8	Mg	dFm	$-CH_3$
57	Cu-dFm-ZIF-8	Cu	dFm	$-CH_3$
58	dIm-ZIF-8	Zn	dIm	$-CH_3$
59	Co-dlm-ZIF-8	Co	dIm	$-CH_3$
60	Be-dlm-ZIF-8	Be	dIm	$-CH_3$
61	Cu-dlm-ZIF-8	Cu	dIm	$-CH_3$
62	Mg-dlm-ZIF-8	Mg	dIm	$-CH_3$
63	dBrm-ZIF-8	Zn	dBrm	$-CH_3$
64	Co-dBrm-ZIF-8	Co	dBrm	$-CH_3$
65	Be-dBrm-ZIF-8	Be	dBrm	$-CH_3$
66	Cd-dBrm-ZIF-8	Cd	dBrm	$-CH_3$
67	Mg-dBrm-ZIF-8	Mg	dBrm	$-CH_3$
68	Cu-dBrm-ZIF-8	Cu	dBrm	$-CH_3$

69	ZIF-8-CHO	Zn	mIm	-CHO

2. Simulations

2.1. Force fields

The force fields of for the ZIF interactions have been developed with the use of density functional theory computations (DFT) and can be found in our previous work.[1]

The force field used consists of the following terms: bond stretching (Eq. 1), bond angle bending (Eq. 2) and torsional angle distortion (Eq. 3) for the bonded intra-molecular interactions, as well as Lennard Jones (LJ) and electrostatic terms, for the non-bonded intra- and inter-molecular interactions (Eq. 4):

$$U^{stretch}(l) = \frac{k_l}{2}(l - l_0)^2 \quad (1)$$

$$U^{bend}(\theta) = \frac{k_\theta}{2}(\theta - \theta_0)^2 \quad (2)$$

$$U^{torsion}(\varphi) = k_\varphi\left[1 + cos(m\varphi - \varphi_0)\right] \quad (3)$$

$$U(r_{ij}) = 4\varepsilon_{ij}\left[\left(\frac{\sigma_{ij}}{r_{ij}}\right)^{12} - \left(\frac{\sigma_{ij}}{r_{ij}}\right)^{6}\right] + \frac{1}{4\pi\varepsilon_0}\frac{q_i q_j}{r_{ij}} \quad (4)$$

where k_l, k_θ and k_φ are constants that characterize the bond length, bond angle and torsional angle stiffness, respectively; l, θ and φ correspond to the bond length, bond angle and torsional angle, respectively, and subscript 0 refers to the equilibrium value; ε_{ij} and σ_{ij} are the Lennard-Jones energy and size parameters, r_{ij} is the distance between atoms i and j, q_i is the charge at atom i and ε_0 is the permittivity of vacuum.

The force-field development has presented in our previous work.[1]

2.2. Simulations in the ZIFs

Each modification was reconstructed on the molecular level, in the form of a super-cell, which corresponds to a box of (2×2×2) unit cells. Then, each ZIF variant underwent equilibration with Molecular Dynamics (MD) simulations, at the NPT ensemble, at 308 K and 1 bar for 1 ns, in order to allow for correct framework volume adjustment. The importance of applying an MD simulation at the NPT ensemble prior to the main simulations should be underlined because each new replacement unit affects the framework's volume, which in turn can affect the resulting aperture size. Thus, considering a common volume value across the different ZIF simulation boxes would be incorrect. Then, the structures underwent a similar thermal equilibration, at the NVT ensemble (again at 308 K) for 1 ns. The thermostat in all simulations was Nose-Hoover and the time step was set to 1fs.

2.2.1. dcTST

Conventional MD methods cannot predict diffusivities lower than 10^{-12} m^2/sec,[2] and the non-conventional approach of dcTST had to be used in our case, where in a lot of systems the observed diffusivities were considerably below than this limit. In dcTST diffusivity is approached as a success of "hops" of a molecule under investigation from cage to cage, by crossing the framework's apertures. Numerous attempts lead to a successful aperture crossing, and the success rate can be translated to the diffusivity, through the following expression:

$$D_0 = \frac{1}{2n} k_{EXIT} l^2 \qquad (5)$$

where n depends on the dimensionality of diffusion, which in ZIF-8 equals to 3, k_{EXIT} is the total exiting rate of a molecule from a cage to any of the adjacent ones, and l is the distance between energy minima, which are the centers of cages (for example, this distance in ZIF-8 is 14 Å).

The total exiting rate is estimated by:

$$k_{EXIT} = n_{apertures} k_{crossing} = 8 k_{crossing} \qquad (6)$$

Where $n_{apertures}$ is the number of available exiting apertures in a cage (8 in SOD topology) and $k_{crossing}$ is the rate of successful crossings of a molecule through a given aperture, through

$$k_{crossing} = \frac{1}{\sqrt{2\pi m}} P(\lambda^*) \qquad (7)$$

where m is the mass of the molecule under investigation, λ is the reaction coordinate and can be regarded as a function of the Cartesian coordinates (see Figure S3(b)). $P(\lambda^*)$ is the probability of finding the molecule in the dividing surface, which is an orthogonal plane at $\lambda = \lambda^*$ vertical to the reaction axis, close to the energy barrier (or at the point free energy is maximized). In our case, the energy barrier corresponds to the aperture's center. The probability $P(\lambda^*)$ depends on the free energy barrier and is obtained from:

$$P(\lambda^*) = \sqrt{\frac{k_B T}{2\pi m}} \frac{e^{-\beta F(\lambda^*)}}{\int_{-\infty}^{\lambda^*} e^{-\beta F(\lambda)}} \tag{8}$$

where F stands for the free energy and it is provided by the umbrella sampling analysis discussed above.

The crossing rate, $k_{crossing}$, of equation 7 does not account for some seemingly successful jumps failing to thermalize in the new cage that end up back again to the cage they came from.[3] To account for this, a dynamic correction factor must be calculated, called correction factor (κ). Thus, the actual, crossing rate is:

$$k_{crossing}^{dc} = \kappa k_{crossing} \tag{9}$$

The probability, $P(\lambda^*)$, in equation 8, is estimated with the help of umbrella sampling.[4] Details on the umbrella sampling and the estimation of the correction factor can be found in our previous work.[5]

2.2.2. Solubilities with test particle insertion

In test particle insertion a single molecule is introduced in a ZIF, at different directions and positions, in numerous ZIF configurations that have been produced beforehand through MD simulations, in the isochoric-isothermal (N,V,T) ensemble. Then, the excess chemical potential of component i is calculated through:[6]

$$\mu_i^{ex} = -\frac{1}{\beta} \ln \left[\left\langle \exp\left(-\beta U_{test}^{inter} \right) \right\rangle_{Widom,N,V,T} \right] \tag{10}$$

where $\beta = 1/k_B T$ and U_{test}^{inter} is the intermolecular energy of the inserted gas molecule, due to its interaction with the surrounding ZIF atoms. The averaging indicated by the brackets is carried out over all the degrees of freedom of the inserted gas molecule and all ZIF conformations. For each ZIF under study, 1000 different structure configurations were produced with MD simulations and in each configuration a single gas molecule is inserted 50,000 times. The solubility, S_i, of species i, is given by:[6]

$$S_i = \frac{22400 cm^3(STP)}{mol} \frac{1}{RT} exp\left(-\frac{\mu_i^{ex}}{RT}\right) \quad (11)$$

Finally, the permeability of species i can be calculated through:

$$P_i = D_i \times S_i \quad (12)$$

3. AI tools development: Machine Learning and Genetic Algorithms

3.1. Table with all available building units considered in our algorithm

The descriptors of the ML models were based on readily-available information about the linkers, functional groups and the metal center of each ZIFs, as well as information about the guest molecules, that does not require additional calculations from a potential user of our tool, such as potential energy surfaces.[7,8] Sixteen descriptors (ML features) were used for ZIFs (Table S2): linker length (×3), linker mass (×3), and ε and σ of the outermost atoms of the linker forming the apertures bridging the cages; the length and mass of the functional groups (×3); the radius and the atomic number of the metal. For the gas molecules (Table S3), the descriptors were: van der Waals and kinetic diameter, mass and acentric factor.

Table S2. ZIF descriptors in our ML models.

Building unit	Descriptors
Metal	Atomic Num.
	Radius
Linker 1	Length
	Mass

	Sigma
	Epsilon
Linker 2	Length
	Mass
	Sigma
	Epsilon
Linker 3	Length
	Mass
	Sigma
	Epsilon
Func. group 1	Length
	Mass
Func. group 2	Length
	Mass
Func. group 3	Length
	Mass

Table S3. Gas descriptors in our ML models.

Descriptors
van der Waals diameter
Kinetic diameter
Mass
Ascentric factor

Table S4. Linkers

	Length (Å)	Mass (u)	σ (Å)	e (kJ/mol)
Imidazolate	4.438	81	0.25	0.0627
bIm	5.996	117	0.25	0.0627
Tetrazolate	3.66	83	0.325	0.7112
dClm	5.7	134.9	0.34	1.2552
dFm	4.86	101.98	0.285	0.255
dBrm	6.010	223.8	0.4	1.8731

dIm	6.410	317.8	0.367	2.4267

Table S5. Functional groups

	Length (Å)	Mass(u)
$-CH_3$	3.78	15
-Br	3.85	79.9
-Cl	3.54	35.45
-H	2.278	1
$-NH_2$	3.927	16
-CHO	4.093	31

Table S6. Metals

	Ionic Radius (pm)	Metal Number	Metal Mass (u)
Cd^{2+}	92	48	112.41
Zn^{2+}	74	30	65.38
Cu^{2+}	71	29	63.456
Co^{2+}	72	27	58.93
Be^{2+}	41	4	9.012
Mg	71	12	24.305
Mn	80	25	54.938

3.2. Details on the gas molecules considered.

Table S7. The gas molecules considered, along with their properties.

	Mass	vdW diameter[9]	Kinetic diameter[9]	Acentric factor[10]

	(g/mol)	(Å)	(Å)	
He	4.00	2.66	2.60	-0.390
H_2	2.01	2.76	2.89	-0.217
O_2	32.00	2.94	3.46	0.022
CO_2	44.01	3.24	3.30	0.225
N_2	28.00	3.13	3.64	0.037
CH_4	16.04	3.25	3.80	0.011
C_2H_4	28.05	3.59	3.90	0.087
C_2H_6	30.07	3.72	4.00	0.099
Kr	83.8	4.00	3.69	0.005
Xe	131.29	4.1	4.1	0.008
C_3H_6	42.08	4.03	4.50	0.142
C_3H_8	44.10	4.16	4.30	0.152
Rn	222	4.2	4.2	0.008
n-C_4H_{10}	58.12	4.52	4.50	0.200
i-C_4H_{10}	58.12	4.80	4.42	0.183

3.3. Details on the ML models

3.3.1. The Dataset

The dataset used in the training of the ML models is an extended version of a dataset we published recently.[1] It consists of ZIFs that we manually designed and equilibrated with molecular simulations, with force fields developed in house. More specifically:

1. The training dataset in the present publication misses the three designed ZIFs (for the three separations). These ZIFs with the guidance of our GA tool in the original dataset.
2. The training dataset in the present publication is extended in the sense that we expanded the range of the gas molecules. We carried out simulations for the diffusivity calculation for Kr, Xe and Rn (additionally to the gas molecules included in the original dataset).

3.3.2. The ML models

Scikit learn was used for the ML models. The parameters for the various regressors are supplied in Table S8.

Table S8. Information on the ML regressors of our work.

Regressor type	Parameters
LR	None
DT	*Max depth*: 6
RF	*Max depth*: 6, *n_estimators* = 600
NN	*Layers*: (50, 30, 30, 20, 10); *solver*: lbfgs; *max_iter* = 5000
GP	*Kernel = ConstantKernel(1.0, (10^{-2}, 10^{3}))×DotProduct(5, (10^{-7}, 10^{3}))×RBF(5, (10^{-7}, 10^{3}))* *M_restarts_optimizier=20, alpha=0.01, normalize_y=True*
GBR	*n_estimators* = 500; *learning_rate* = 0.2; *max_depth*=6; *loss*='squared_error'
XGBR	*n_estimators*=500; *max_depth*=5; *eta*=0.07; *subsample*=0.75, *colsample_bytree*=0. 7, reg_lambda=0.4, reg_alpha=0.13

The performance of the Ml models, as shown in the plot of Figure 1, in the main text, was accomplished by using the *K*-fold cross-validation protocol:[11] the set is split randomly in *K* folds, that do not overlap. One of the folds is the test set, and the rest are used to train the models. This procedure is repeated, until all folds have served as the test set. The metrics used were R^2, med absolute (ABS) error, mean squared error (MSE), the maximum error and mean ABS perc error. The performance is shown in the following Table:

Table S9. Performance metrics of the various ML models developed in this work.

	R^2	Med ABS error	Max error	Mean ABS error	MSE
LR	0.761	1.726	19.181	0.167	7.861
DT	0.890	0.851	10.049	0.089	3.635
RF	0.925	0.764	6.857	0.075	2.485
NN	0.919	0.610	9.092	0.072	2.680

GBR	0.984	0.337	5.442	0.037	0.550
XGBR	0.985	0.290	6.5	0.030	0.528

3.4. Details on our genetic algorithm

3.4.1. Genetic algorithm development

The development of the genetic algorithm was based on the PyGAD library.[12]

Parent selection

For the parent selection we chose the K tournament method, while the crossover type was set to uniform. Six (6) parents mated at each generation, which were selected through the K tournament method, with K_tournament = 12.

K_tournament = 12

The 4 best candidates at the end of each generation run were kept in the population (keep_eliticism). The crossover probability was 0.7.

Mutation

Most importantly, we used the adaptive mutation,[13] which avoids the pits of the total randomness of mutation, by promoting the evolution of high quality genes and discouraging the transfer of "bad" genes to the next generations. The mutation probabilities were 0.6 for solutions whose performance was below the population average performance, and 0.06 for solutions whose performance was above the population average performance.

Number of generations

In the case of the O_2/N_2, 3000 generation steps were used. For the design of optimum ZIF for CO_2/CH_4 and C_3H_6/C_3H_8, where our algorithm's design was limited to symmetrical ZIFs, the number of generation steps was reduced to 100.

3.4.2. The three ZIFs

In the case of O_2/N_2, the GA algorithm could freely construct ZIFs of independent linker and functional group composition. In the case of ZIFs designed for CO_2/CH_4 and C_3H_6/C_3H_8 separations, we limited the ZIF generation routine in our GA algorithm, to construct symmetrical ZIFs (linker1=linker2=linker3; functional_group_1=functional_group_2=functional_group_3),

because the search space gets rapidly crowded by proposed optimized structures for the given performance boundaries.

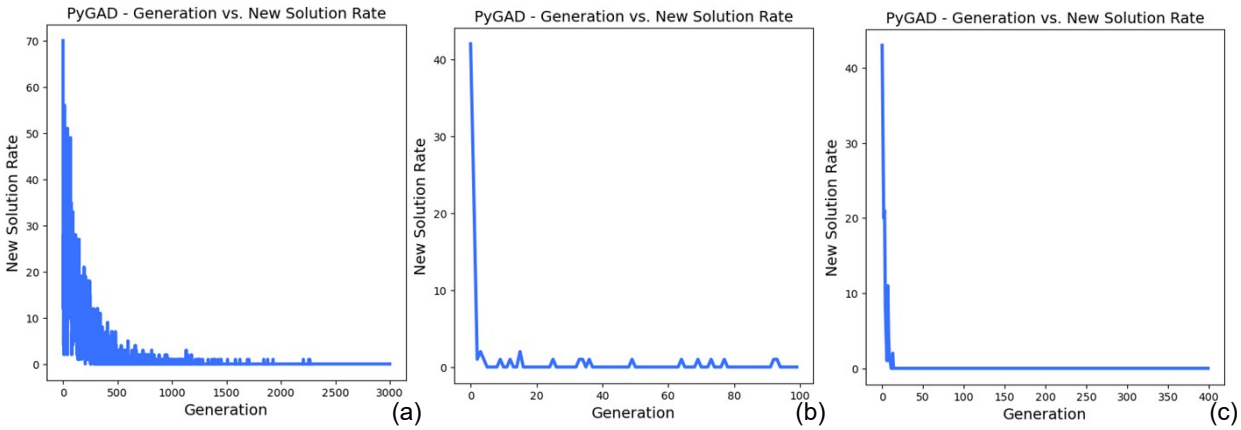

Figure S1. New solutions rate as a function of the generation number for the case of (a) O_2/N_2, (b) CO_2/CH_4, and (c) C_3H_6/C_3H_8.

Table S10. Simulation results

ZIF	gas	D (m^2/s)	S ($cm^3(STP)/cm^3cmHg$)	Permeability (Barrer)
Cd-I-ZIF-7-8	O_2	1.2×10^{-12}	5.3×10^{-2}	6.57
	N_2	5.8×10^{-14}	5.1×10^{-2}	0.12
dFmBe	CO_2	6.6×10^{-10}	0.5	1.1×10^{4}
	CH_4	1.0×10^{-14}	0.24	0.24
ZIF-67	C_3H_6	2.0×10^{-13}	5.2	154.71
	C_3H_8	1.5×10^{-15}	9.2	1.38

Table S11. Literature data in Figures 1 and 3(a) (CO_2/CH_4)

membrane	P_{CO2} (Barrer)	P_{CO2}/P_{CH4}
ZIF-8[14]	7.16×10^3	5.1
ZIF-8 (31%)/P84[15]	20	95
Matrimid®-PEG[16]/ZIF-8 (4%)	27.5	24
PDMS/ACN-O (10%)[17]	4.3×10^3	4.5
PVC-g-POEM[18]	43.5	18.1
PVC-g-POEM/H-ZIF 5%[18]	51.7	17.2
PVC-g-POEM/H-ZIF 10%[18]	210.6	14.3
PVC-g-POEM/H-ZIF 20%[18]	224.7	11.9
P84/ND[19]	1.61	75
Matrimid/ZIF-1 (10%)[20]	6.75	23
6FDA-TTM/Si-H (5%)[21]	29.7	76
MWCNT@GONRs (2%)[22]	25.2	11
LOYMET[23]	29	31.74
KIOJUQ[23]	478	22.34
15wt% ZIF-90B/6FDA-DAM[24]	720	37
PIM-EA(H_2)-TB[25]	1.4×10^3	17.7
MOF@COF/PSf-5 MMM[26]	7	50
NH2-MIL-53(Al)[27]	53	28.7
PVC-g-POEM/H_ZIF-8[28]	62.3	11.2
SSZ-13[29]	6×10^3	300
Matrimids-CNTs/GO-5/5[30]	38	85
VAD-OS-SAPO-34[31]	4.3×10^3	158
Matrimid/UiO-67-33[32]	27	75
6FDA-DAM/UiO-66-$COCH_3$[33]	1.2×10^3	33
Pebax®-P84®[34]	19	114
Pebax®-P84®-ZIF-8[34]	19	65
Pebax®-P84®-MIL-101[34]	19	60
Pebax®-P84®-UiO-66[34]	29	56
Pebax®-P84®-ZIF-7/8[34]	18	50
CHA S-L-18[35]	2×10^3	30
PIM-BTrip[36]	1×10^4	25.6
PIM-DM-BTrip[36]	1.3×10^4	20
PIM-DTFM-BTrip[36]	1.7×10^4	18.7
PIM-DM-BTrip[36]	16×10^4	16.5
PIM-DM-BTrip[36]	23×10^4	13.2
PIM-TMN-Trip[36]	23×10^4	15.7
PIM-TFM-BTrip[36]	33×10^4	14.7
Pebax/ZIF-8[37]	118	21
Pebax/ZIF-67[37]	162	25
ZIF-7[38]	5.6	13
IRMOF-1[39]	1.1×10^4	328

DD3R[40] (zeolite)	3.8×10^3	590
SAPO-34[41] (zeolite)	2.99×10^3	115
ALPO-18[42] (zeolite)	1.97×10^3	59.2
T[43] (zeolite)	2.75×10^3	400
ZIF-62 glass[44]	2.64×10^3	36
CAU-1-NH_2/organosilica[45]	1.07×10^5	18
SIM-1[46]	2.6×10^3	1.1
Bio-MOF-1[47]	5.4×10^4	2.6
Sod-ZMOF-1[48]	94	3.6
Bio-MOF-1[49]	16.57	42.6
MnP3nF7[50]	16.48	82.4
Matrimid/NiDOBDC/GO[51]	10	58.3
PSM-MOF[52]	1.89×10^3	17.7
PEBA/CuBTC[53]	96.2	23.1
Polymer/NH_2-ZIF-8[54]	218	13.84
Pebax®1657 UiO-66-NH_2[55]	97.5	22.1
Pebax®1657 UiO-66[55]	118.3	30.5
Pebax®1657 ZIF-8[56]	758	16.1
Pebax®1657 CuBTC[57]	56.2	23.4
Pebax®2533 ZIF-11[58]	402.89	12.49
Polysulfone ZIF-8[59]	12.1	19.8
Polysulfone $Mn(HCOO)_2$[60]	6.83	9.16
Polysulfone $Cu_3(BTC)_2$[60]	304.4	3.6
Polysulfone MIL-101[61]	32.0	23.50
Pebax®1657 MIL-53(Al)[62]	129	23.3
Pebax®1657 NH_2-MIL-53(Al) [62]	149	20.5
Pebax ZIF-67 NP[63]	95.7	12.9
Pebax ZIF-67 MP[63]	101	12.8
Pebax Zif-67 NS[63]	139	17.6
Pebax MH 1657 a-Ni$(im)_2$[64]	100.6	33.4
Pebax®1657/SAPO-34 (50%)[65]	338	16
Pebax/UiO-66-NH_2[66]	845	20
Pebax/UiO-66[66]	562.5	16
Pebax/UiO-66-$(COOH)_2$[66]	600	17.5
PSf/NH_2-MIL-53(Al)[67]	6	47
PSf/NH_2-MIL-53(Al)[68]	4.5	26
PVDF/ NH_2-MIL-53(Al)[69]	1.4×10^3	26.03
PI/ NH_2-MIL-53(Al)[70]	8.5	44
PMP/ NH_2-MIL-53(Al)[70]	339.5	22.8
PI/ NH_2-MIL-53(Al)[71]	9.2	2.1
Ultem/ NH_2-MIL-53(Al)[71]	3	36.1
Matrimid/ NH_2-MIL-53(Al)[72]	7.5	42
Matrimid/ NH_2-MIL-53(Al)[73]	6.6	19.2
Matrimid/ NH_2-MIL-53(Al)[73]	2.8	82
Matrimid/ NH_2-MIL-53(Al)[73]	3.8	94
Matrimid/ NH_2-MIL-53(Al)[73]	1.7	139

Matrimid/ZIF-7[74]	4.5	155
Matrimid/ Ni_2(dobdc)[75]	14.7	32.5
Matrimid/ZIF-8[76]	12.96	41.5
Pebax 1675/CuNi[77]	70.9	18.65
PEEK-WC/CuNi[77]	47.84	47.84
6FDA-mPD/MOF-199[78]	50	89
6FDA-BI[79]	9	75.3
P/Zn^{2+}[79]	9.1	79.8
6FDA-BI/20%ZIF-8[79]	20.3	57.9
6FDA-BI/20%ZIF-8 0.004 Zn^{2+}[79]	22.8	60.3
6FDA-BI/20%ZIF-8 0.007 Zn^{2+}[79]	27.4	56.1
6FDA-BI/20%ZIF-8 0.01 Zn^{2+}[79]	15.9	70.2
P84 - $[Ni_3(HCOO)_6]$[80]	1	62
	1.3	67
PN10[81]	96.2	22.9
PN20[81]	145	25.4
PN30[81]	264	27.9
PN40[81]	395	36.3
PPO/ZIF-8 (3 wt%)[82]	76.1	18.1
PPO/ZIF-8 (6 wt%)[82]	75.3	17.7
PPO/ZIF-8 (10 wt%)[82]	99.5	17.3
PPO/ZIF-8 (15 wt%)[82]	114.1	17.3
PPO/ZIF-8 (25 wt%)[82]	189	15.9
PPO/ZIF-8 (35 wt%)[82]	314.2	16.6
PPO/ZIF-8 (45 wt%)[82]	448.7	11.8
ZIF-S[83]	2802	21.01
ZIF-S[83]	3390.7	16.92
ZIF-S[83]	3762.34	17.35
ZIF-S[83]	3809	14.23
ZIF-S[83]	4219.9	12.62
ZIF-S[83]	4517.1	12.5
Pebax ZIF-8 3%[84]	169.719	19.105
Pebax Zif-8 10%[84]	174.37	19.187
Pebax ZIF-8 20%[84]	198.55	15.056
PIM-1/ZIF-7[85]	3640	16.6
PIM-1/NH_2-ZIF-7[85]	2948	20.7
PMP/Pebax/CNF-UiO[86]	186.9	16.5
PMP/Pebax/CNF-UiO[86]	220.4	21.1
CuBTC-PVDF 0%[87]	0.9115	21.27
CuBTC-PVDF 5%[87]	1.067	24.81
CuBTC-PVDF 10%[87]	2.002	41.7
CuBTC-PVDF 15%[87]	3.206	40.07
CuBDC-PVDF 5%[87]	1.126	26.18
CuBDC-PVDF10%[87]	1.602	35.6
CuBDC-PVDF15%[87]	1.987	45.15
MIL-53(Al) 5%[87]	1.21	21.22

MIL-53(Al) 10%[87]	1.553	20.98
NH2-MIL-53(Al) 5%[87]	1.107	23.06
NH2-MIL-53(Al) 10%[87]	1.406	26.03
MIL-101(Cr)-SPEEK[87]	31	31
MIL-101(Cr)-SPEEK[87]	29	29
MIL-101(Cr)-SPEEK[87]	1623	33
MIL-101(Cr)-SPEEK[87]		
Commercialy attractive region by: Hilock et al.[88]	33.7	35.1

Table S12. Literature data in Figure 3(b) (O_2/N_2)

membrane	P_{O2} (Barrer)	P_{O2}/P_{N2}
ZIF-8[89]	7.32×10^3	2.71
ZIF-8-poly(1,4-phelyene ether-ether-sulfone)[90]	10.65	5.33
Polyurethane – ZSM-5[91]	21.5	2.7
PIM-SBF[92]	1.87×10^3	3.4
PIM-1[93]	600	4.8
PSF – P (0.5 μm)[94]	30	1.8
PSF – P (10 μm)[94]	70	7
PSF-3PDMS[95]	82.5	4.6
PIM-1A/NanoMIL-101[96]	3×10^3	3
Matrimid®5218/PIM-EA(H_2)-TB[25]	350	5.6
Matrimid®-ZIF-8[97]	5.6	6.4
poly(Pn4)[98]	494	2.2
PIM-TMN-Trip[36]	152	6.4
PIM-HMI-Trip[36]	706	4.9
PIM-DM-BTrip[36]	1.3×10^3	4.5
PIM-DTFM-BTrip[36]	1.9×10^3	3.5
PIM-TFM-BTrip[36]	3×10^3	3.8
	63	6.5
2abIm-VPLT-LIPS-ZIF-8[99]	111	5.7
	218	5.9
Sod-ZMOF-1[48]	18.5	1.7
PSM-MOF[52]	310	2.84
Pebax 1675/CuNi[77]	3.8	2.71
PEEK-WC/CuNi[77]	6.51	4.93
Pebax ZIF-8 3%[84]	7.261	1.791
Pebax Zif-8 10%[84]	8.929	2.109
Pebax ZIF-8 20%[84]	11.314	2.349
MOF-801/PIM-1[100]	1752	4.8
Commercially attractive region by:		

Zhang et al.[101]	0.83	8.2

Bibliography

(1) Krokidas, P.; Karozis, S.; Moncho, S.; Giannakopoulos, G.; Brothers, E. N.; Kainourgiakis, M. E.; Economou, I. G.; Steriotis, T. A. Data Mining for Predicting Gas Diffusivity in Zeolitic-Imidazolate Frameworks (ZIFs). *J. Mater. Chem. A* **2022**, *10*, 13697–13703.

(2) Gulbalkan, H. C.; Haslak, Z. P.; Altintas, C.; Uzun, A.; Keskin, S. Assessing CH4/N2 Separation Potential of MOFs, COFs, IL/MOF, MOF/Polymer, and COF/Polymer Composites. *Chem. Eng. J.* **2022**, *428*, 131239.

(3) June, R. L.; Bell, A. T.; Theodorou, D. N. Transition-State Studies of Xenon and Sulfur Hexafluoride Diffusion in Silicalite. *J. Phys. Chem.* **1991**, *95*, 8866–8878.

(4) Kästner, J. Umbrella Sampling. *Wiley Interdiscip. Rev. Comput. Mol. Sci.* **2011**, *1*, 932–942.

(5) Krokidas, P.; Moncho, S.; Brothers, E. N.; Economou, I. G. Defining New Limits in Gas Separations Using Modified ZIF Systems. *ACS Appl. Mater. Interfaces* **2020**, *12*, 20536–20547.

(6) Raptis, V. E.; Economou, I. G.; Theodorou, D. N.; Petrou, J.; Petropoulos, J. H. Molecular Dynamics Simulation of Structure and Thermodynamic Properties of Poly(Dimethylsilamethylene) and Hydrocarbon Solubility Therein: Toward the Development of Novel Membrane Materials for Hydrocarbon Separation. *Macromolecules* **2004**, *37*, 1102–1112.

(7) Bucior, B. J.; Bobbitt, N. S.; Islamoglu, T.; Goswami, S.; Gopalan, A.; Yildirim, T.; Farha, O. K.; Bagheri, N.; Snurr, R. Q. Energy-Based Descriptors to Rapidly Predict Hydrogen Storage in Metal-Organic Frameworks. *Mol. Syst. Des. Eng.* **2019**, *4*, 162–174.

(8) Halder, P.; Singh, J. K. High-Throughput Screening of Metal-Organic Frameworks for Ethane-Ethylene Separation Using the Machine Learning Technique. *Energy and Fuels* **2020**, *34*, 14591–14597.

(9) Zhang, C.; Lively, R. P.; Zhang, K.; Johnson, J. R.; Karvan, O.; Koros, W. J. Unexpected Molecular Sieving Properties of Zeolitic Imidazolate Framework-8. *J. Phys. Chem. Lett.* **2012**, *3*, 2130–2134.

(10) *Perry's Chemical Engineers' Handbook*, 9th editio.; Green, D. W., Southard, M. Z., Eds.; McGraw-Hill Education: New York, 2019.

(11) Hastie, T.; Tibshirani, R.; Friedman, J. *The Elements of Statistical Learning: Data Mining, Inference, and Prediction, Second Edition*; Springer, 2016.

(12) Gad, A. F. PyGAD: An Intuitive Genetic Algorithm Python Library. *arXiv* **2021**.

(13) Marsili Libelli, S.; Alba, P. Adaptive Mutation in Genetic Algorithms. *Soft Comput.* **2000**, *4*, 76–80.

(14) Venna, S. R.; Carreon, M. A. Highly Permeable Zeolite Imidazolate Framework-8 Membranes for CO 2/CH4 Separation. *J. Am. Chem. Soc.* **2010**, *132*, 76–78.

(15) Guo, A.; Ban, Y.; Yang, K.; Yang, W. Metal-Organic Framework-Based Mixed Matrix Membranes : Synergetic Effect of Adsorption and Diffusion for CO2 / CH4 Separation. *J. Memb. Sci.* **2018**, *562*, 76–84.

(16) Castro-Muñoz, R.; Fíla, V.; Martin-Gil, V.; Muller, C. Enhanced CO2permeability in Matrimid® 5218 Mixed Matrix Membranes for Separating Binary CO2/CH4mixtures. *Sep. Purif. Technol.* **2019**, *210*, 553–562.

(17) Heidari, M.; Hosseini, S. S.; Omidkhah Nasrin, M. R.; Ghadimi, A. Synthesis and Fabrication of Adsorptive Carbon Nanoparticles (ACNs)/PDMS Mixed Matrix Membranes for Efficient CO2/CH4and C3H8/CH4separation. *Sep. Purif. Technol.* **2019**, *209*, 503–515.

(18) Lee, J. H.; Kwon, H. T.; Bae, S.; Kim, J.; Kim, J. H. Mixed-Matrix Membranes Containing Nanocage-like Hollow ZIF-8 Polyhedral Nanocrystals in Graft Copolymers for Carbon Dioxide/Methane Separation. *Sep. Purif. Technol.* **2018**, *207*, 427–434.

(19) Pulyalina, A.; Polotskaya, G.; Rostovtseva, V.; Pientka, Z.; Toikka, A. Improved Hydrogen Separation Using Hybrid Membrane Composed of Nanodiamonds and P84 Copolyimide. *Polymers (Basel).* **2018**, *10*, 828.

(20) Safak Boroglu, M.; Yumru, A. B. Gas Separation Performance of 6FDA-DAM-ZIF-11 Mixed-Matrix Membranes for H2/CH4and CO2/CH4separation. *Sep. Purif. Technol.* **2017**, *173*, 269–279.

(21) Lanč, M.; Sysel, P.; Šoltys, M.; Štěpánek, F.; Fónod, K.; Klepić, M.; Vopička, O.; Lhotka,

M.; Ulbrich, P.; Friess, K. Synthesis, Preparation and Characterization of Novel Hyperbranched 6FDA-TTM Based Polyimide Membranes for Effective CO2separation: Effect of Embedded Mesoporous Silica Particles and Siloxane Linkages. *Polymer (Guildf).* **2018**, *144*, 33–42.

(22) Xue, Q.; Pan, X.; Li, X.; Zhang, J.; Guo, Q. Effective Enhancement of Gas Separation Performance in Mixed Matrix Membranes Using Core/Shell Structured Multi-Walled Carbon Nanotube/Graphene Oxide Nanoribbons. *Nanotechnology* **2017**, *28*, 65702–65712.

(23) Altintas, C.; Keskin, S. Molecular Simulations of MOF Membranes and Performance Predictions of MOF/Polymer Mixed Matrix Membranes for CO 2 /CH 4 Separations. *ACS Sustain. Chem. Eng.* **2019**, *7*, 2739–2750.

(24) Bae, T. H.; Lee, J. S.; Qiu, W.; Koros, W. J.; Jones, C. W.; Nair, S. A High-Performance Gas-Separation Membrane Containing Submicrometer-Sized Metal-Organic Framework Crystals. *Angew. Chemie - Int. Ed.* **2010**, *49*, 9863–9866.

(25) Esposito, E.; Mazzei, I.; Monteleone, M.; Fuoco, A.; Carta, M.; McKeown, N. B.; Malpass-Evans, R.; Jansen, J. C. Highly Permeable Matrimid®/PIM-EA(H2)-TB Blend Membrane for Gas Separation. *Polymers (Basel).* **2018**, *11*, 1–14.

(26) Cheng, Y.; Ying, Y.; Zhai, L.; Liu, G.; Dong, J.; Wang, Y.; Christopher, M. P.; Long, S.; Wang, Y.; Zhao, D. Mixed Matrix Membranes Containing MOF@COF Hybrid Fillers for Efficient CO 2 /CH 4 Separation. *J. Memb. Sci.* **2019**, *573*, 97–106.

(27) Mubashir, M.; Yeong, Y. F.; Lau, K. K.; Chew, T. L.; Norwahyu, J. Efficient CO2/N2 and CO2/CH4 Separation Using NH2-MIL-53(Al)/Cellulose Acetate (CA) Mixed Matrix Membranes. *Sep. Purif. Technol.* **2018**, *199*, 140–151.

(28) Hwang, S.; Chi, W. S.; Lee, S. J.; Im, S. H.; Kim, J. H.; Kim, J. Hollow ZIF-8 Nanoparticles Improve the Permeability of Mixed Matrix Membranes for CO2/CH4 Gas Separation. *J. Memb. Sci.* **2015**, *480*, 11–19.

(29) Zheng, Y.; Hu, N.; Wang, H.; Bu, N.; Zhang, F.; Zhou, R. Preparation of Steam-Stable High-Silica CHA (SSZ-13) Membranes for CO2/CH4 and C2H4/C2H6 Separation. *J. Memb. Sci.* **2015**, *475*, 303–310.

(30) Li, X.; Ma, L.; Zhang, H.; Wang, S.; Jiang, Z.; Guo, R.; Wu, H.; Cao, X. Z.; Yang, J.; Wang,

B. Synergistic Effect of Combining Carbon Nanotubes and Graphene Oxide in Mixed Matrix Membranes for Efficient CO2 Separation. *J. Memb. Sci.* **2015**, *479*, 1–10.

(31) Mu, Y.; Chen, H.; Xiang, H.; Lan, L.; Shao, Y.; Fan, X.; Hardacre, C. Defects-Healing of SAPO-34 Membrane by Post-Synthesis Modification Using Organosilica for Selective CO 2 Separation. *J. Memb. Sci.* **2019**, *575*, 80–88.

(32) Thür, R.; Van Velthoven, N.; Slootmaekers, S.; Didden, J.; Verbeke, R.; Smolders, S.; Dickmann, M.; Egger, W.; De Vos, D.; Vankelecom, I. F. J. Bipyridine-Based UiO-67 as Novel Filler in Mixed-Matrix Membranes for CO2-Selective Gas Separation. *J. Memb. Sci.* **2019**, *576*, 78–87.

(33) Ahmad, M. Z.; Navarro, M.; Lhotka, M.; Zornoza, B.; Téllez, C.; de Vos, W. M.; Benes, N. E.; Konnertz, N. M.; Visser, T.; Semino, R.; et al. Enhanced Gas Separation Performance of 6FDA-DAM Based Mixed Matrix Membranes by Incorporating MOF UiO-66 and Its Derivatives. *J. Memb. Sci.* **2018**, *558*, 64–77.

(34) Sánchez-Laínez, J.; Gracia-Guillén, I.; Zornoza, B.; Téllez, C.; Coronas, J. Thin Supported MOF Based Mixed Matrix Membranes of Pebax® 1657 for Biogas Upgrade. *New J. Chem.* **2019**, *43*, 312–319.

(35) Karakiliç, P.; Wang, X.; Kapteijn, F.; Nijmeijer, A.; Winnubst, L. Defect-Free High-Silica CHA Zeolite Membranes with High Selectivity for Light Gas Separation. *J. Memb. Sci.* **2019**, *586*, 34–43.

(36) Comesaña-Gándara, B.; Chen, J.; Bezzu, C. G.; Carta, M.; Rose, I.; Ferrari, M.-C.; Esposito, E.; Fuoco, A.; Jansen, J. C.; McKeown, N. B. Redefining the Robeson Upper Bounds for CO 2 /CH 4 and CO 2 /N 2 Separations Using a Series of Ultrapermeable Benzotriptycene-Based Polymers of Intrinsic Microporosity . *Energy Environ. Sci.* **2019**, *12*, 2733–2740.

(37) Meshkat, S.; Kaliaguine, S.; Rodrigue, D. Comparison between ZIF-67 and ZIF-8 in Pebax® MH-1657 Mixed Matrix Membranes for CO2 Separation. *Sep. Purif. Technol.* **2020**, *235*, 116150.

(38) Cacho-Bailo, F.; Catalán-Aguirre, S.; Etxeberría-Benavides, M.; Karvan, O.; Sebastian, V.; Téllez, C.; Coronas, J. Metal-Organic Framework Membranes on the Inner-Side of a Polymeric Hollow Fiber by Microfluidic Synthesis. *J. Memb. Sci.* **2015**, *476*, 277–285.

(39) Rui, Z.; James, J. B.; Kasik, A.; Lin, Y. S. Metal-Organic Framework Membrane Process for High Purity CO2 Production. *AIChE J.* **2016**, *62*, 3836–3841.

(40) van den Bergh, J.; Zhu, W.; Gascon, J.; Moulijn, J. A.; Kapteijn, F. Separation and Permeation Characteristics of a DD3R Zeolite Membrane. *J. Memb. Sci.* **2008**, *316*, 35–45.

(41) Li, S.; Falconer, J. L.; Noble, R. D. Improved SAPO-34 Membranes for CO2/CH4 Separations. *Adv. Mater.* **2006**, *18*, 2601–2603.

(42) Carreon, M. L.; Li, S.; Carreon, M. A. AlPO-18 Membranes for CO2/CH4 Separation. *Chem. Commun.* **2012**, *48*, 2310–2312.

(43) Cui, Y.; Kita, H.; Okamoto, K. I. Preparation and Gas Separation Performance of Zeolite T Membrane. *J. Mater. Chem.* **2004**, 924–932.

(44) Wang, Y.; Jin, H.; Ma, Q.; Mo, K.; Mao, H.; Feldhoff, A.; Cao, X.; Li, Y.; Pan, F.; Jiang, Z. A MOF Glass Membrane for Gas Separation. *Angew. Chemie - Int. Ed.* **2020**, *59*, 4365–4369.

(45) Kong, C.; Du, H.; Chen, L.; Chen, B. Nanoscale MOF/Organosilica Membranes on Tubular Ceramic Substrates for Highly Selective Gas Separation. *Energy Environ. Sci.* **2017**, *10*, 1812–1819.

(46) Aguado, S.; Nicolas, C. H.; Moizan-Baslé, V.; Nieto, C.; Amrouche, H.; Bats, N.; Audebrand, N.; Farrusseng, D. Facile Synthesis of an Ultramicroporous MOF Tubular Membrane with Selectivity towards CO2. *New J. Chem.* **2011**, *35*, 41–44.

(47) Bohrman, J. A.; Carreon, M. A. Synthesis and CO2/CH4 Separation Performance of Bio-MOF-1 Membranes. *Chem. Commun.* **2012**, *48*, 5130–5132.

(48) Al-Maythalony, B. A.; Shekhah, O.; Swaidan, R.; Belmabkhout, Y.; Pinnau, I.; Eddaoudi, M. Quest for Anionic MOF Membranes: Continuous Sod -ZMOF Membrane with Co2 Adsorption-Driven Selectivity. *J. Am. Chem. Soc.* **2015**, *137*, 1754–1757.

(49) Ishaq, S.; Tamime, R.; Bilad, M. R.; Khan, A. L. Mixed Matrix Membranes Comprising of Polysulfone and Microporous Bio-MOF-1: Preparation and Gas Separation Properties. *Sep. Purif. Technol.* **2019**, *210*, 442–451.

(50) Rajati, H.; Navarchian, A. H.; Rodrigue, D.; Tangestaninejad, S. Improved CO2 Transport

Properties of Matrimid Membranes by Adding Amine-Functionalized PVDF and MIL-101(Cr). *Sep. Purif. Technol.* **2019**, *235*, 116149.

(51) Li, W.; Chuah, C. Y.; Nie, L.; Bae, T. H. Enhanced CO 2 /CH 4 Selectivity and Mechanical Strength of Mixed-Matrix Membrane Incorporated with NiDOBDC/GO Composite. *J. Ind. Eng. Chem.* **2019**, *74*, 118–125.

(52) Qian, Q.; Wu, A. X.; Chi, W. S.; Asinger, P. A.; Lin, S.; Hypsher, A.; Smith, Z. P. Mixed-Matrix Membranes Formed from Imide-Functionalized UiO-66-NH2 for Improved Interfacial Compatibility. *ACS Appl. Mater. Interfaces* **2019**, *11*, 31257–31269.

(53) Erfani, A.; Asghari, M. Comparison of Micro- and Nano-Sized CuBTC Particles on the CO2/CH4 Separation Performance of PEBA Mixed Matrix Membranes. *J. Chem. Technol. Biotechnol.* **2020**, *n/a*.

(54) Raza, A.; Farrukh, S.; Hussain, A.; Khan, I. U.; Noor, T.; Othman, M. H. D.; Yousaf, M. F. Development of High Performance Amine Functionalized Zeolitic Imidazolate Framework (ZIF-8)/Cellulose Triacetate Mixed Matrix Membranes for CO2/CH4 Separation. *Int. J. Energy Res.* **2020**, *44*, 7989–7999.

(55) Sarmadi, R.; Salimi, M.; Pirouzfar, V. The Assessment of Honeycomb Structure UiO-66 and Amino Functionalized UiO-66 Metal–Organic Frameworks to Modify the Morphology and Performance of Pebax®1657-Based Gas Separation Membranes for CO2 Capture Applications. *Environ. Sci. Pollut. Res.* **2020**.

(56) Jomekian, A.; Behbahani, R. M.; Mohammadi, T.; Kargari, A. CO2/CH4 Separation by High Performance Co-Casted ZIF-8/Pebax 1657/PES Mixed Matrix Membrane. *J. Nat. Gas Sci. Eng.* **2016**, *31*, 562–574.

(57) Khosravi, T.; Omidkhah, M. Preparation of CO2 Selective Composite Membranes Using Pebax/CuBTC/PEG-Ran-PPG Ternary System. *J. Energy Chem.* **2017**, *26*, 530–539.

(58) Ehsani, A.; Pakizeh, M. Synthesis, Characterization and Gas Permeation Study of ZIF-11/Pebax® 2533 Mixed Matrix Membranes. *J. Taiwan Inst. Chem. Eng.* **2016**, *66*, 414–423.

(59) Zornoza, B.; Seoane, B.; Zamaro, J. M.; Téllez, C.; Coronas, J. Combination of MOFs and Zeolites for Mixed-Matrix Membranes. *ChemPhysChem* **2011**, *12*, 2781–2785.

(60) Car, A.; Stropnik, C.; Peinemann, K.-V. Hybrid Membrane Materials with Different Metal–Organic Frameworks (MOFs) for Gas Separation. *Desalination* **2006**, *200*, 424–426.

(61) Tanh Jeazet, H. B.; Koschine, T.; Staudt, C.; Raetzke, K.; Janiak, C. Correlation of Gas Permeability in a Metal-Organic Framework MIL-101(Cr)-Polysulfone Mixed-Matrix Membrane with Free Volume Measurements by Positron Annihilation Lifetime Spectroscopy (PALS). *Membranes (Basel).* **2013**, *3*, 331–353.

(62) Meshkat, S.; Kaliaguine, S.; Rodrigue, D. Mixed Matrix Membranes Based on Amine and Non-Amine MIL-53(Al) in Pebax® MH-1657 for CO2 Separation. *Sep. Purif. Technol.* **2018**, *200*, 177–190.

(63) Feng, S.; Bu, M.; Pang, J.; Fan, W.; Fan, L.; Zhao, H.; Yang, G.; Guo, H.; Kong, G.; Sun, H.; et al. Hydrothermal Stable ZIF-67 Nanosheets via Morphology Regulation Strategy to Construct Mixed-Matrix Membrane for Gas Separation. *J. Memb. Sci.* **2020**, *593*, 117404.

(64) Li, C.; Wu, C.; Zhang, B. Enhanced CO2/CH4 Separation Performances of Mixed Matrix Membranes Incorporated with Two-Dimensional Ni-Based MOF Nanosheets. *ACS Sustain. Chem. & Eng.* **2019**, *8*, 642–648.

(65) Zhao, D.; Ren, J.; Li, H.; Hua, K.; Deng, M. Poly(Amide-6-b-Ethylene Oxide)/SAPO-34 Mixed Matrix Membrane for CO 2 Separation. *J. Energy Chem.* **2014**, *23*, 227–234.

(66) Sutrisna, P. D.; Hou, J.; Zulkifli, M. Y.; Li, H.; Zhang, Y.; Liang, W.; D'Alessandro, D. M.; Chen, V. Surface Functionalized UiO-66/Pebax-Based Ultrathin Composite Hollow Fiber Gas Separation Membranes. *J. Mater. Chem. A* **2018**, *6*, 918–931.

(67) Zornoza, B.; Martinez-Joaristi, A.; Serra-Crespo, P.; Tellez, C.; Coronas, J.; Gascon, J.; Kapteijn, F. Functionalized Flexible MOFs as Fillers in Mixed Matrix Membranes for Highly Selective Separation of CO2 from CH4 at Elevated Pressures. *Chem. Commun.* **2011**, *47*, 9522–9524.

(68) Rodenas, T.; Van Dalen, M.; Serra-Crespo, P.; Kapteijn, F.; Gascon, J. Mixed Matrix Membranes Based on NH2-Functionalized MIL-Type MOFs: Influence of Structural and Operational Parameters on the CO 2/CH4 Separation Performance. *Microporous Mesoporous Mater.* **2014**, *192*, 35–42.

(69) Feijani, E. A.; Mahdavi, H.; Tavasoli, A. Poly(Vinylidene Fluoride) Based Mixed Matrix

Membranes Comprising Metal Organic Frameworks for Gas Separation Applications. *Chem. Eng. Res. Des.* **2015**, *96*, 87–102.

(70) Abedini, R.; Omidkhah, M.; Dorosti, F. Highly Permeable Poly(4-Methyl-1-Pentyne)/NH2-MIL 53 (Al) Mixed Matrix Membrane for CO2/CH4 Separation. *RSC Adv.* **2014**, *4*, 36522–36537.

(71) Chen, X. Y.; Hoang, V.-T.; Rodrigue, D.; Kaliaguine, S. Optimization of Continuous Phase in Amino-Functionalized Metal–Organic Framework (MIL-53) Based Co-Polyimide Mixed Matrix Membranes for CO2/CH4 Separation. *RSC Adv.* **2013**, *3*, 24266–24279.

(72) Sabetghadam, A.; Seoane, B.; Keskin, D.; Duim, N.; Rodenas, T.; Shahid, S.; Sorribas, S.; Guillouzer, C. Le; Clet, G.; Tellez, C.; et al. Metal Organic Framework Crystals in Mixed-Matrix Membranes: Impact of the Filler Morphology on the Gas Separation Performance. *Adv. Funct. Mater.* **2016**, *26*, 3154–3163.

(73) Kertik, A.; Wee, L. H.; Sentosun, K.; Navarro, J. A. R.; Bals, S.; Martens, J. A.; Vankelecom, I. F. J. High-Performance CO2-Selective Hybrid Membranes by Exploiting MOF-Breathing Effects. *ACS Appl. Mater. Interfaces* **2020**, *12*, 2952–2961.

(74) Kertik, A.; Wee, L. H.; Pfannmöller, M.; Bals, S.; Martens, J. A.; Vankelecom, I. F. J. Highly Selective Gas Separation Membrane Using in Situ Amorphised Metal-Organic Frameworks. *Energy Environ. Sci.* **2017**, *10*, 2342–2351.

(75) Bachman, J. E.; Long, J. R. Plasticization-Resistant Ni2(Dobdc)/Polyimide Composite Membranes for the Removal of CO2 from Natural Gas. *Energy Environ. Sci.* **2016**, *9*, 2031–2036.

(76) Zhang, Z.; Xian, S.; Xia, Q.; Wang, H.; Li, Z.; Li, J. Enhancement of CO2 Adsorption and CO2/N2 Selectivity on ZIF-8 via Postsynthetic Modification. *AIChE J.* **2013**, *59*, 2195–2206.

(77) Esposito, E.; Bruno, R.; Monteleone, M.; Fuoco, A.; Soria, J. F.; Pardo, E.; Armentano, D.; Jansen, J. C. Glassy PEEK-WC vs. Rubbery Pebax®1657 Polymers: Effect on the Gas Transport in CuNi-MOF Based Mixed Matrix Membranes. *Appl. Sci.* **2020**, *10*.

(78) Nuhnen, A.; Klopotowski, M.; Tanh Jeazet, H. B.; Sorribas, S.; Zornoza, B.; Téllez, C.; Coronas, J.; Janiak, C. High Performance MIL-101(Cr)@6FDA-: M PD and MOF-

199@6FDA- m PD Mixed-Matrix Membranes for CO2/CH4 Separation. *Dalt. Trans.* **2020**, *49*, 1822–1829.

(79) Fan, Y.; Yu, H.; Xu, S.; Shen, Q.; Ye, H.; Li, N. Zn(II)-Modified Imidazole Containing Polyimide/ZIF-8 Mixed Matrix Membranes for Gas Separations. *J. Memb. Sci.* **2020**, *597*, 117775.

(80) Sheng, L.; Guo, Y.; Zhao, D.; Ren, J.; Wang, S.; Deng, M. Enhanced CO2/CH4 Separation Performance of BTDA-TDI/MDI (P84) Copolyimide Mixed-Matrix Membranes by Incorporating Submicrometer-Sized [Ni3(HCOO)6] Framework Crystals. *J. Nat. Gas Sci. Eng.* **2020**, *75*, 103123.

(81) Habib, N.; Shamair, Z.; Tara, N.; Nizami, A. S.; Akhtar, F. H.; Ahmad, N. M.; Gilani, M. A.; Bilad, M. R.; Khan, A. L. Development of Highly Permeable and Selective Mixed Matrix Membranes Based on Pebax®1657 and NOTT-300 for CO2 Capture. *Sep. Purif. Technol.* **2020**, *234*.

(82) Benedetti, F. M.; De Angelis, M. G.; Degli Esposti, M.; Fabbri, P.; Masili, A.; Orsini, A.; Pettinau, A. Enhancing the Separation Performance of Glassy PPO with the Addition of a Molecular Sieve (ZIF-8): Gas Transport at Various Temperatures. *Membranes (Basel).* **2020**, *10*, 56.

(83) Ye, C.; Wu, X.; Wu, H.; Yang, L.; Ren, Y.; Wu, Y.; Liu, Y.; Guo, Z.; Zhao, R.; Jiang, Z. Incorporating Nano-Sized ZIF-67 to Enhance Selectivity of Polymers of Intrinsic Microporosity Membranes for Biogas Upgrading. *Chem. Eng. Sci.* **2020**, *216*, 115497.

(84) Sutrisna, P. D.; Savitri, E. High Gas Permeability of NanoZIF-8/Polymer-Based Mixed Matrix Membranes Intended for Biogas Purification. *J. Polym. Eng.* **2020**, *40*, 459–467.

(85) Wang, Y.; Ren, Y.; Wu, H.; Wu, X.; Yang, H.; Yang, L.; Wang, X.; Wu, Y.; Liu, Y.; Jiang, Z. Amino-Functionalized ZIF-7 Embedded Polymers of Intrinsic Microporosity Membrane with Enhanced Selectivity for Biogas Upgrading. *J. Memb. Sci.* **2020**, *602*, 117970.

(86) Mozafari, M.; Rahimpour, A.; Abedini, R. Exploiting the Effects of Zirconium-Based Metal Organic Framework Decorated Carbon Nanofibers to Improve CO2/CH4 Separation Performance of Thin Film Nanocomposite Membranes. *J. Ind. Eng. Chem.* **2020**, *85*, 102–110.

(87) Xin, Q.; Liu, T.; Li, Z.; Wang, S.; Li, Y.; Li, Z.; Ouyang, J.; Jiang, Z.; Wu, H. Mixed Matrix Membranes Composed of Sulfonated Poly(Ether Ether Ketone) and a Sulfonated Metal-Organic Framework for Gas Separation. *J. Memb. Sci.* **2015**.

(88) Hillock, A. M. W.; Miller, S. J.; Koros, W. J. Crosslinked Mixed Matrix Membranes for the Purification of Natural Gas: Effects of Sieve Surface Modification. *J. Memb. Sci.* **2008**, *314*, 193–199.

(89) Hara, N.; Yoshimune, M.; Negishi, H.; Haraya, K.; Hara, S.; Yamaguchi, T. Diffusive Separation of Propylene/Propane with ZIF-8 Membranes. *J. Memb. Sci.* **2014**, *450*, 215–223.

(90) Díaz, K.; López-González, M.; Del Castillo, L. F.; Riande, E. Effect of Zeolitic Imidazolate Frameworks on the Gas Transport Performance of ZIF8-Poly(1,4-Phenylene Ether-Ether-Sulfone) Hybrid Membranes. *J. Memb. Sci.* **2011**, *383*, 206–213.

(91) Taheri Afarani, H.; Sadeghi, M.; Moheb, A.; Esfahani, E. N. Optimization of the Gas Separation Performance of Polyurethane–Zeolite 3A and ZSM-5 Mixed Matrix Membranes Using Response Surface Methodology. *Chinese J. Chem. Eng.* **2019**, *27*, 110–129.

(92) Bezzu, C. G.; Carta, M.; Ferrari, M. C.; Jansen, J. C.; Monteleone, M.; Esposito, E.; Fuoco, A.; Hart, K.; Liyana-Arachchi, T. P.; Colina, C. M.; et al. The Synthesis, Chain-Packing Simulation and Long-Term Gas Permeability of Highly Selective Spirobifluorene-Based Polymers of Intrinsic Microporosity. *J. Mater. Chem. A* **2018**, *6*, 10507–10514.

(93) Bernardo, P.; Bazzarelli, F.; Tasselli, F.; Clarizia, G.; Mason, C. R.; Maynard-Atem, L.; Budd, P. M.; Lanč, M.; Pilnáček, K.; Vopička, O.; et al. Effect of Physical Aging on the Gas Transport and Sorption in PIM-1 Membranes. *Polymer (Guildf).* **2017**, *113*, 283–294.

(94) Prajapati, P. K.; Kansara, A. M.; Singh, P. S. Preparation and Characterization of an Oxygen Permselective Polydimethylsiloxane Hollow Fibre Membrane. *RSC Adv.* **2016**, *6*, 88943–88953.

(95) Ismail, A.; Chong, K.; Roslan, R.; Lau, W.; Thiam, H.; Lai, S. Preparation, Characterization, and Performance Evaluation of Polysulfone Hollow Fiber Membrane with PEBAX or PDMS Coating for Oxygen Enhancement Process. *Polymers (Basel).* **2018**, *10*, 126.

(96) Khdhayyer, M.; Bushell, A. F.; Budd, P. M.; Attfield, M. P.; Jiang, D.; Burrows, A. D.;

Esposito, E.; Bernardo, P.; Monteleone, M.; Fuoco, A.; et al. Mixed Matrix Membranes Based on MIL-101 Metal–Organic Frameworks in Polymer of Intrinsic Microporosity PIM-1. *Sep. Purif. Technol.* **2019**, *212*, 545–554.

(97) Song, Q.; Nataraj, S. K.; Roussenova, M. V.; Tan, J. C.; Hughes, D. J.; Li, W.; Bourgoin, P.; Alam, M. A.; Cheetham, A. K.; Al-Muhtaseb, S. A.; et al. Zeolitic Imidazolate Framework (ZIF-8) Based Polymer Nanocomposite Membranes for Gas Separation. *Energy Environ. Sci.* **2012**, *5*, 8359–8369.

(98) Zang, Y.; Aoki, T.; Shoji, K.; Teraguchi, M.; Kaneko, T.; Ma, L.; Jia, H.; Miao, F. Synthesis and Oxygen Permeation of Novel Well-Defined Homopoly(Phenylacetylene)s with Different Sizes and Shapes of Oligosiloxanyl Side Groups. *J. Memb. Sci.* **2018**, *561*, 26–38.

(99) Eum, K.; Hayashi, M.; De Mello, M. D.; Xue, F.; Kwon, H. T.; Tsapatsis, M. ZIF-8 Membrane Separation Performance Tuning by Vapor Phase Ligand Treatment. *Angew. Chemie Int. Ed.* **2019**, *58*, 1–5.

(100) Chen, W.; Zhang, Z.; Hou, L.; Yang, C.; Shen, H.; Yang, K.; Wang, Z. Metal-Organic Framework MOF-801/PIM-1 Mixed-Matrix Membranes for Enhanced CO2/N2 Separation Performance. *Sep. Purif. Technol.* **2020**, *250*, 117198.

(101) Zhang, B.; Wang, T.; Zhang, S.; Qiu, J.; Jian, X. Preparation and Characterization of Carbon Membranes Made from Poly(Phthalazinone Ether Sulfone Ketone). *Carbon N. Y.* **2006**, *44*, 2764–2769.